*Environ. Sci. Technol.* **1998**, *32,* 2308−2316

# Laboratory Development of Permeable Reactive Mixtures for the Removal of Phosphorus from Onsite Wastewater Disposal Systems

MICHAEL J. BAKER,* DAVID W. BLOWES, AND CAROL J. PTACEK

*Department of Earth Sciences, University of Waterloo, Waterloo, Ontario N2L 3G1, Canada*

Laboratory batch and column studies were conducted to develop permeable reactive mixtures to remove phosphorus from the effluent of onsite wastewater disposal systems. Mixtures can be placed in situ, as horizontal or vertical reactive barriers in sediments receiving wastewater discharge, or can be used in single pass, self-contained treatment modules in alternative treatment systems. Reactive mixtures composed of silica sand, high calcium crushed limestone, and readily available metal oxides were tested to evaluate phosphorus attenuation. Iron/calcium oxides, produced from steel manufacturing, and fine-grained activated aluminum oxide outperformed other oxides tested during batch experiments. These materials removed greater than 99% of $PO_4$ from a 10 mg/L $PO_4$−P solution within 1 h of contact. Long-term attenuation capacities of the mixtures were assessed by continually loading bench-scale columns with a 3.3 mg/L $PO_4$−P solution, at representative groundwater flow rates. A column containing 50 wt % silica sand, 45 wt % limestone, and 5 wt % iron/calcium oxide averaged >90% reduction in phosphate over 4 years (≈1450 pore volumes). X-ray and SEM microprobe analyses of the reacted solids showed phosphorus accumulations on the surfaces of iron oxide phases and discrete precipitates of microcrystalline hydroxyapatite [$Ca_5(PO_4)_3$-OH]. A second column containing 50 wt % silica sand, 40 wt % limestone, and 10 wt % activated aluminum oxide achieved >99% reduction in $PO_4$ over a period of 2 years (≈413 pore volumes). The treatment performance in this system can be attributed to the high adsorption capacity of the aluminum oxide.

## Introduction

Approximately one-third of the population of North America utilizes onsite wastewater disposal systems for pretreatment and disposal of domestic wastewater. Conventional septic systems provide primary wastewater treatment anaerobically in a septic tank, followed by aerobic treatment in an unsaturated soil absorption bed. Primary wastewater treatment lowers the biological oxygen demand, decreases suspended solids, removes or filters out pathogenic microbes and bacteria, and converts ammonia to nitrate (*1, 2*). These systems, however, often do not completely remove nutrients, such as phosphorus. Field studies have determined that long-term wastewater disposal can deplete natural attenuation capacities, leading to phosphorus mobility in groundwater (*3, 4*). Phosphorus is the limiting nutrient controlling productivity in most inland, freshwater systems (*5*). Surface waters receiving excess inputs of nutrients through wastewater discharges may be susceptible to eutrophication.

It is desirable, in some cases, to augment onsite wastewater disposal systems with phosphorus treatment capabilities. The requirements for implementation of phosphorus treatment are that the approach is economically and technically compatible with current onsite designs, capable of providing effective long-term treatment, and not maintenance intensive. Brooks et al. (*6*) introduced sphagnum peat filters as an alternative method of primary wastewater treatment in addition to some N and P removal. Chowdry (*7*) describes a sand filter media mixed with red mud through which domestic effluent is passed to promote the adsorption of phosphorus onto metal oxides. P removal in this system, however, was found to steadily decrease over time, presumably due to the finite adsorption capacity of the red mud.

An adaptation to the red mud−sand filter concept is permeable reactive mixtures that simultaneously promote both adsorption of phosphate on metal oxides and precipitation of sparingly soluble phosphate mineral phases (*8, 9*). A reactive mixture can be placed as a horizontal treatment layer within conventional septic system tile beds (Figure 1A). For alternative onsite systems [e.g., recirculating sand filters (*10*), aerobic biofilters (*11*)], the reactive mixture can be incorporated as a self-contained, single pass flow-through module after primary treatment and before final disposal (Figure 1B). In situations where phosphate plumes have the potential to impact sensitive environments, a vertical in situ treatment barrier can be installed (Figure 1C). The primary benefits of the system are that it can achieve desired levels of phosphorus attenuation regardless of site conditions and effectively accumulate phosphorus in a finite and accessible volume of material. This material is available for future collection and disposal if necessary or, in special cases, acceptable rates of phosphorus release.

Surfaces of metal oxides are important $PO_4$ adsorption sites due to the presence of a multiply charged cation, high positive surface charge densities at near-neutral pH, and the propensity to hydroxylate in aqueous systems. $PO_4$ adsorption is described as specific adsorption through ligand exchange with surface hydroxyl groups forming stable, inner-sphere surface complexes (*12*). This reaction permits adsorption of the $PO_4$ anion to occur even under relatively high pH conditions, where mineral surfaces may possess net negative surface charges. The orthophosphate anion can also combine with cations to form stable, sparingly soluble $PO_4$ mineral phases (*13*). Therefore, a potentially effective reactive mixture is one that provides a geochemical environment that promotes both adsorption and precipitation reactions.

The objectives of this study are to quantify the potential treatment capabilities of reactive mixtures containing both high calcium limestone and readily available metal oxides and to determine the importance of adsorption and precipitation reactions as potential treatment mechanisms. Short-term batch experiments were used as an efficient method of comparing phosphate removal rates of a range of reactive materials. Optimal mixtures were selected for dynamic column experiments to assess the long-term attenuation capacities under conditions of continuous phosphate loading.

* Corresponding author Fax: (519)746-3882; e-mail: blowes@sciborg.uwaterloo.ca.


S0013-936X(97)00934-6 CCC: $15.00 
Published on Web 06/27/1998

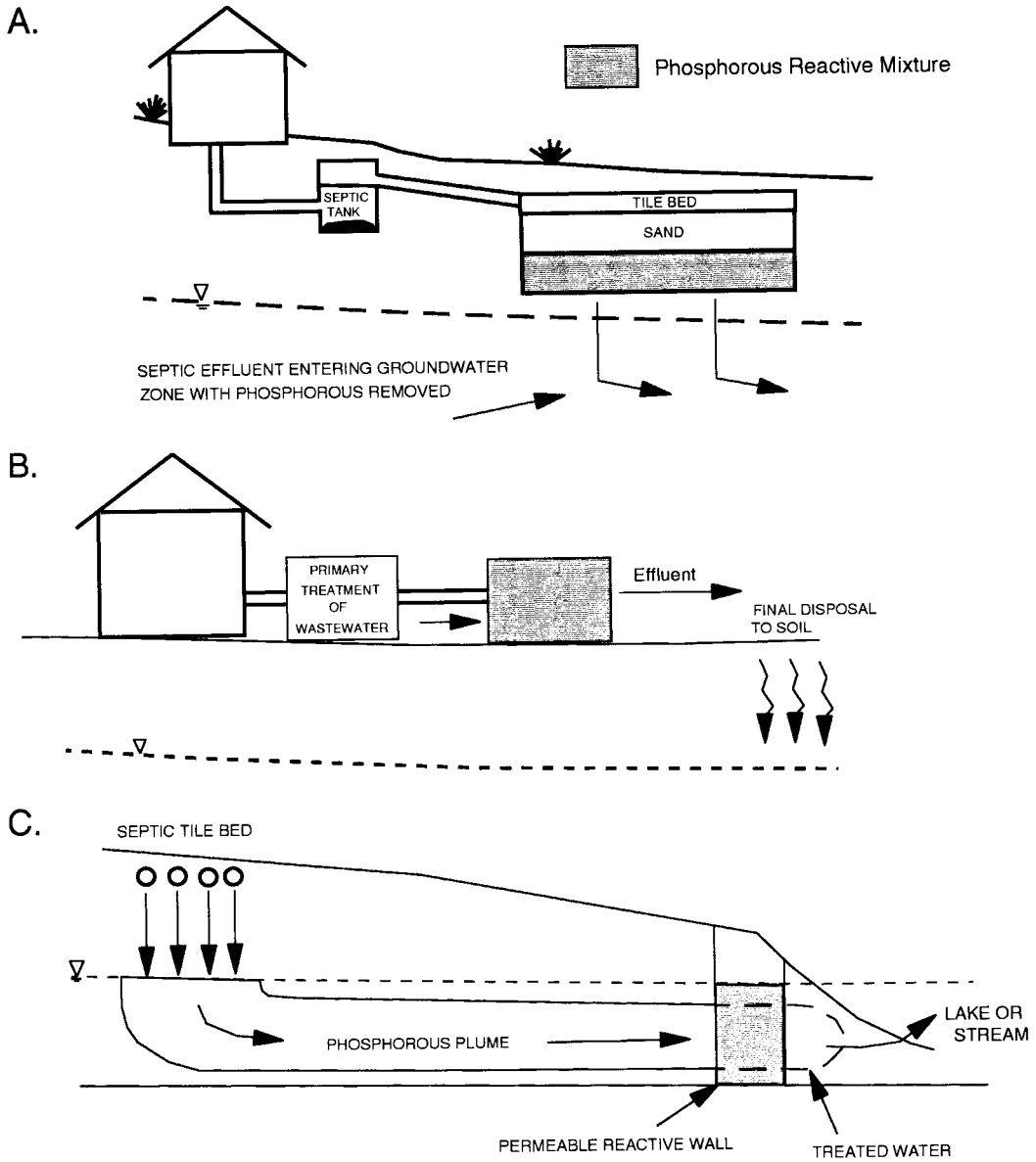


**FIGURE 1. Schematic of phosphorus reactive mixture applied to onsite wastewater disposal systems.**

## Methodology

**Description of Materials.** The reactive mixtures tested contained three components. The first component was a metal oxide with characteristics suitable for specific $PO_4$ adsorption. The second component was crushed, high calcium limestone to provide a long-term calcium source, pH conditions, and reactive surfaces necessary for calcium phosphate precipitation. The third component, silica sand, provides a permeable matrix for the overall mixture. The source of silica sand and limestone remained constant in this study. Iron and aluminum oxides with different chemical, mineralogical, and physical characteristics were obtained from a variety of sources.

Seven iron oxides were tested (Table 1). Four were obtained as byproducts of steel manufacturing. The crystal form of the iron oxide is dependent on the manufacturing process and typically contains additional elements in various oxide and silicate forms. Together the integrated steel manufacturers of Canada produce over 4 million ton of iron oxide waste annually (*14*). Pure, synthetic forms of the three principle iron oxide mineral phases (goethite, hematite, and magnetite) also were tested. Six commercially available aluminum oxide materials were tested (Table 1). These materials included aluminum hydrate, activated alumina, and calcined alumina. Red mud, the primary waste byproduct from aluminum refineries, was also tested. As a comparison, natural calcareous and noncalcareous aquifer sands were also examined in batch experiments (Table 1).

**Batch Experiments.** Reactive mixtures tested contained 50 wt % silica sand, 45 wt % crushed limestone, and 5 wt % metal oxide. A total of 50 g of dry solids was placed in a 500-mL Erlenmeyer glass flask. A 500-g stock phosphate solution (approximately 10 mg/L $PO_4$−P) was prepared by dissolving $KH_2PO_4$ salt in double deionized water. The solid:solution mass ratio of 50 g of solids:500 g of solution allowed time-dependent observations in variations in $PO_4$ concentration. Maximum reaction time for all of the batch tests was limited to 10 h. The $PO_4$ solution was added to the reaction flask, and the flask was sealed and placed on an orbital shaker to bring the mixture into suspension. A polyethylene plastic syringe was used to extract a 30-mL aliquot of solution, which was filtered through a 0.45-$\mu$m syringe filter for $PO_4$−P and pH determinations. Analyses of orthophosphate were performed using the ascorbic acid colorimetric technique (*15*) with a Shimadzu spectrophotometer. Measurements of pH were made with an Accumet

**TABLE 1. Description of Solid Materials Used During Laboratory Experiments[a]**

| material | chemical composition | dominant mineralogy | grain size range (mm) | surface area ($m^2/g$) | comments |
|---|---|---|---|---|---|
| | | **Reference Materials** | | | |
| quartz sand | Si | $SiO_2$ | 0.59−0.84 | − | − |
| limestone | Si | $CaCO_3$, $MgCO_3$ | − | − | high calcium, crushed agricultural limestone (>97% $CaCO_3$) |
| noncalcareous sand | Si | quartz, feldspar | 0.75[c] | − | natural aquifer sand |
| calcareous sand | Si | quartz, feldspar, cacite | 0.2[c] | − | natural aquifer sand |
| | | **Iron Oxides** | | | |
| BOF-oxide | Fe, Ca, Mg, Mn, Si, Zn | $Fe_3O_4$, $Fe_2O_3$, $Ca(OH)_2$, $CaCO_3$ | 0.003−0.1 | 4.5−4.7 | byproduct of steel manufacturing |
| BOF-slag | Ca, Fe, Mg, Mn, Si, Al | $Ca_2SiO_4$, $Ca(OH)_2$, FeO, $CaFe_2O_4$ | 0.84 | − | byproduct of steel manufacturing |
| OG-sludge | Fe | − | − | − | byproduct of steel manufacturing |
| BF-sludge | Fe | − | − | − | byproduct of steel manufacturing |
| magnetite | Fe | $Fe_3O_4$ | 0.0003 | 8.0 | synthetically prepared pure phase |
| goethite | Fe | FeOOH | 0.0005 | 16.4 | synthetically prepared pure phase |
| hematite | Fe | $Fe_2O_3$ | 0.00015 | 15.0 | synthetically prepared pure phase |
| | | **Aluminum Oxides** | | | |
| red mud | Al, Fe, Si, Ca | sodium/aluminum silicates, $Fe_2O_3$ | − | − | principle waste product of bauxite refineries |
| AA300G | Al | $\gamma$-$Al_2O_3$ | 1.0−1.4 | 350−380 | activated alumina |
| AA400G | Al | $\gamma$-$Al_2O_3$ | 0.35−0.71 | 350−380 | activated alumina |
| AA100 | Al | $\chi$-$Al_2O_3$ | 0.074−0.088 | 260−280 | activated alumina |
| C-70 | Al | $\alpha$-$Al_2O_3$ | 0.044−0.149 | 0.6 | calcined alumina |
| C-30 | Al | $Al(OH)_3$ | 0.044−0.149 | 0.1 | aluminum hydrate |

[a] Characteristics of the metal oxides provided by the manufacturers. [b] (−), information not available. [c] Grain size of aquifer sands given as the mode of the cumulative distribution.

combination gel electrode standardized with pH 4, 7, and 10 buffer solutions.

**Column Experiments.** Bench-scale columns were designed to ensure uniform saturated flow over the cross-sectional area of the column. Solutions were administered continually through Teflon tubing connected to a multichannel variable-speed Ismatic peristaltic pump. To verify uniform flow conditions in the columns and to determine effective transport porosities, tracer tests were conducted by adding a known concentration of $Cl^-$ to the saturating solution and collecting samples with an automated fraction collector.

A phosphate breakthrough experiment was conducted for each column. An influent solution (≈3.3 mg/L $PO_4$−P) was prepared by dissolving reagent-grade $KH_2PO_4$ salt in double deionized $H_2O$. This concentration was selected based on field observations of $PO_4$ concentrations underlying septic system tile beds (*3*). During routine monitoring, column effluent samples were collected in 60-mL plastic syringes, and flow rates were determined gravimetrically. An unfiltered aliquot of the sample was transferred to a separate vessel for pH determination. The remaining sample was filtered through a 0.45-$\mu$m syringe filter, and total alkalinity measurements were made by titrating with 0.16 N $H_2SO_4$ using a Hach digital titrator. The remaining sample was transferred to 25-mL polyethylene scintillation vials and refrigerated at 4 °C for $PO_4$ analyses. The effluent solution from column 1 was collected periodically for major and minor ion analyses. Filtered−acidified and filtered−unacidified samples were collected and analyzed for Ca, Mg, Na, K, Si, Fe, Mn, Al, Cu, Zn, $SO_4$, Cl, $PO_4$−P, and other trace elements.

Samples of the reactive mixture in column 1 were collected during two separate events to determine the total phosphorus content and for mineralogical study. The column end plates were removed, and 1−1.5 cm of material was extracted from each end of the column with a spatula. The solids were immediately washed in reagent-grade methanol and allowed to air-dry. Dried samples were transferred to sealed plastic containers and stored at room temperature. The volume of material removed from the column was replaced with an equivalent volume of silica sand, resulting in a net reduction of the effective treatment length of the reactive mixture in the column from 20 cm to ≈17 cm. Total phosphorus of each sample was determined by ignition (550 °C) and HCl extraction (50 mL of 1 N HCl with 0.5 g of sample and 24 h contact time) (*16*). The remaining fraction was used for mineralogical study. Polished thin sections were prepared from the bulk sample and examined by optical microscopy using transmitted-light and reflected-light techniques. X-ray diffractometry was performed on powdered mounts with a Rigaku diffractometer using Cu radiation. Microbeam methods included scanning electron microscopy (SEM) using a JEOL 820 instrument coupled with energy dispersion for elemental analyses and a JEOL 733 microprobe with the capacity for energy dispersion and wavelength quantitative analyses. Individual grains of interest were extricated from the polished sections under the microscope and mounted under a petrographic/metallographic microscope and identified using Debye−Scherrer 57.3 mm cameras and Co radiation.

## Results and Discussion

**Batch Experiments.** The input solutions used during the batch experiments contained 10 ± 2 mg/L $PO_4$−P, and the solutions were slightly acidic (pH 5.5−6.0). Concentration versus time profiles for the batch tests are shown in Figure 2. Silica sand did not decrease $PO_4$ concentrations and did not change the pH of the solution and therefore does not contribute to the performance of the reactive mixtures. Noncalcareous aquifer sand demonstrated little pH buffering capacity and removed 13% of the initial $PO_4$. Calcareous aquifer sand buffered the solution pH to ≈8.1 and removed 41% of the initial $PO_4$ over a 10-h period. The mixture containing 50 wt % silica sand and 50 wt % crushed limestone removed 88% of the $PO_4$, and the pH increased to a maximum of 9.1. The interaction between calcite and phosphate has

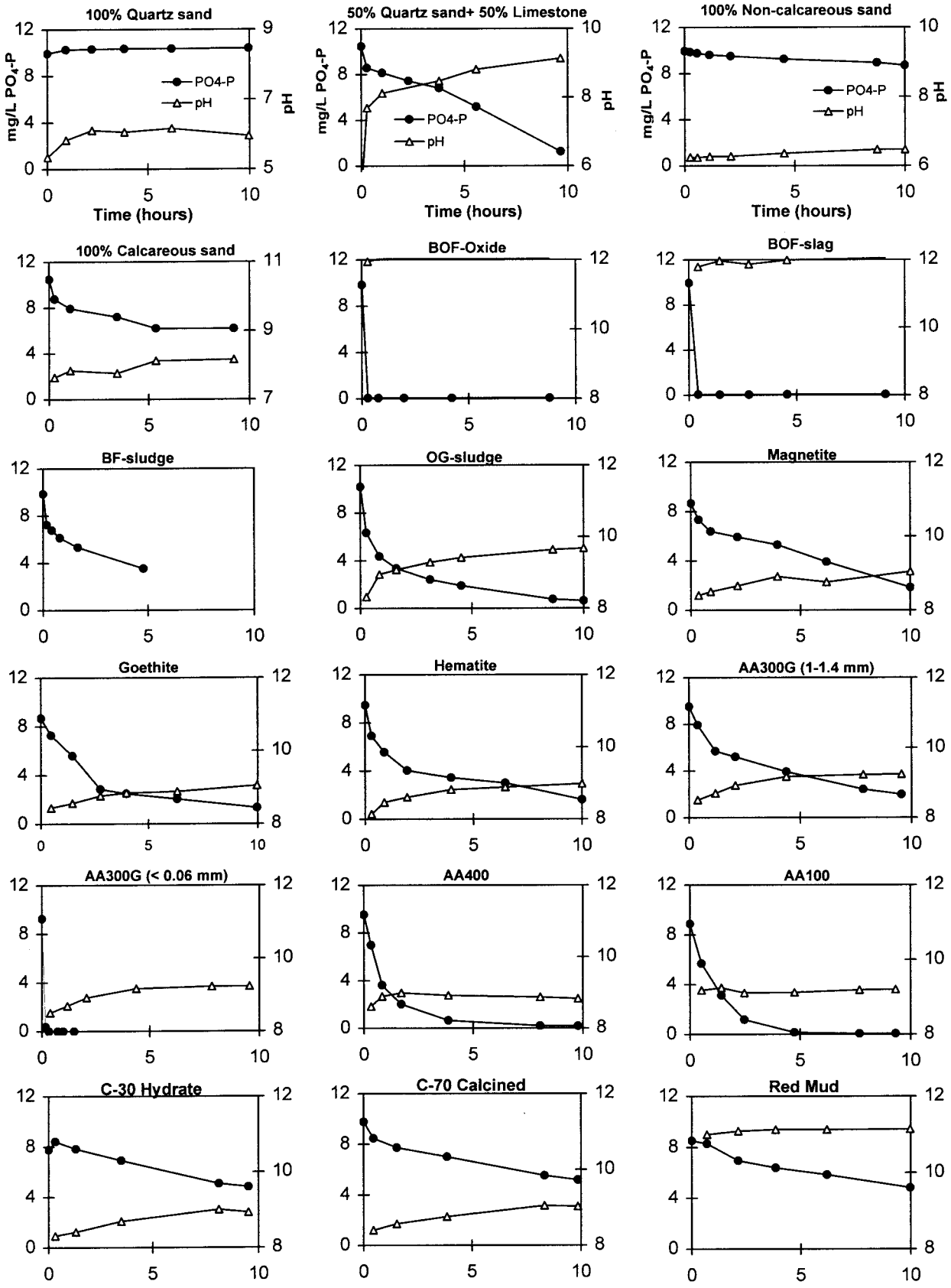


**FIGURE 2. Batch test results. Mixtures contain 50 wt % silica sand, 45 wt % limestone, and 5 wt % oxide (unless otherwise noted).**

been described as monolayer adsorption on only a small percentage of the calcite surface, which can be followed by nucleation and precipitation of calcium phosphate under saturated conditions (*17*). The solutions in contact with limestone are expected to be supersaturated with respect to calcium phosphate given its low solubility under alkaline pH conditions; however, this was not determined during the batch tests. Limestone, therefore, contributes significantly to phosphate attenuation of the reactive mixtures. The resulting increase in pH is expected to reduce the adsorption

affinities of the metal oxides by creating more negative surface charges.

**Reactive Mixtures (Iron Oxides).** The response of the reactive mixtures during the batch experiments varied depending on the specific type of metal oxide used (Figure 2). The results were compared by dividing the total percent reduction in $PO_4$ concentration by the total time of contact. The relative effectiveness of the iron oxides decreased in the order:

$$\text{BOF-oxide} = \text{BOF-slag} \gg \text{OG-sludge} > \text{BF-sludge} > \text{goethite} > \text{hematite} > \text{magnetite}$$

Iron oxide byproducts from steel manufacturing demonstrated strong potential for use in phosphorus treatment. Basic oxygen furnace (BOF) materials (BOF-oxide, BOF-slag) were more effective than blast furnace materials (BF-sludge, OG-sludge). BOF-oxide and BOF-slag removed all phosphate from the batch solutions (<0.01 mg/L $PO_4$−P) within 1.0 h of contact. Although both materials showed a similar response, they are chemically, mineralogically, and physically different. BOF-oxide is a partially oxidized, chemically complex, iron oxide containing significant amounts of Fe, Ca, and Mg in the form of magnetite, hematite, portlandite, calcite, and periclase with a very fine particle size distribution (98 wt % < 25 $\mu$m) (*14*). BOF-slag is a more homogeneous, less oxidized, coarse-grained material containing high concentrations of Ca (portlandite, calcium oxides/silicates), Fe (FeO, ferrites, silicates), Mg, Si, and Al in various oxide and silicate forms (*14*). The only major mineral phase common to both materials is portlandite. The dissolution of portlandite can be expressed as

$$Ca(OH)_2(s) \leftrightarrow Ca^{2+} + 2OH^- \quad (1)$$

The dissolution of portlandite results in a significant increase in pH (≈12) and increased Ca concentrations in the batch solutions. Anion adsorption capabilities of metal oxides present would be expected to be significantly inhibited under such high pH conditions. Therefore, the efficient phosphate uptake observed with BOF iron oxide materials may be attributed more to the extremely low solubility of calcium phosphate under high pH conditions rather than adsorption on metal oxides.

The rate of $PO_4$ removal using pure iron oxides was significantly less than for the steel foundry oxides. Reactive mixtures containing goethite, hematite, and magnetite were compared at pH 8−9. Goethite removed phosphate more rapidly than hematite. The mixture incorporating magnetite did not demonstrate any additional P removal capabilities over the silica sand and limestone mixture.

**Reactive Mixtures (Aluminum Oxides).** Phosphate treatment efficiencies for the aluminum oxides decreased in the order (Figure 2)

$$\text{AA100} > \text{AA400G} > \text{AA300G} > \text{C-70} > \text{C-30} > \text{red mud}$$

All of the experiments using aluminum oxides were performed under similar pH conditions (pH 8−9), controlled by dissolution of the limestone. The pH of the batch solution using red mud was high (pH ≈ 11) due to its alkaline nature. Activated alumina has significantly greater adsorption capabilities than aluminum hydrate and calcined alumina. Activated alumina is a physically and chemically stable form of porous, dehydrated aluminum oxide ($Al_2O_3$) with extremely high surface areas and internal porosity (Table 1), making them ideal adsorbents. Use of activated alumina in fluidized beds has been suggested as a method of phosphorus treatment in municipal wastewater treatment plants (*18*). Smaller particles of activated alumina adsorbed a greater amount of phosphate at a faster rate (e.g., AA300G, Figure 2) due to enhanced exposure of adsorption sites. Phosphate removal observed with the reactive mixture containing red mud was limited to 43% as compared with >99% achieved with fine-grained activated aluminum.

**Column Experiments.** Two separate reactive mixtures (one containing BOF iron oxide, and the other containing AA400G aluminum oxide) were selected for bench-scale dynamic column experiments based on their performance during the batch tests.

Solute transport through each column is expressed as normalized concentration ($C/C_o$) versus normalized time [number of pore volumes (pv)], where $C$ is the effluent concentration, $C_o$ is the average influent concentration over the experiment, and 1 pore volume = $nV_t$, where $n$ is the effective pore volume (pv) calculated from the tracer experiments and $V_t$ is the total volume of the column. Transport parameters from the chloride tracer tests were evaluated using CXTFIT (*19*), a nonlinear, least-squares inversion program that fits experimental data to the advection−dispersion equation.

**Column 1.** The mixture in column 1 contained 50 wt % silica sand, 45 wt % high calcium, crushed limestone, and 5 wt % BOF oxide. Two tracer experiments were conducted, one at the beginning and one at the end of the 4-year study period. Both Cl breakthrough curves were in good agreement, indicating no significant loss of porosity within the column. An average porosity of 0.24 (pore volume = 152 $cm^3$) was selected as most representative. On the basis of the calculated porosity, velocities averaged 24.9 ± 6.3 cm/day, corresponding to a dimensionless flow rate of 1.3 ± 0.3 pore volume/day and an average residence time in the column of 0.9 ± 0.2 day.

A $KH_2PO_4$ orthophosphate input solution was continually administered to the column for a total time of 4.0 years (1450 pore volumes). The input solution averaged 3.31 ± 0.09 mg/L $PO_4$−P ($n$ = 43), and the measured pH varied between 5.3 and 5.6. Breakthrough curves for $PO_4$ and pH are shown in Figure 3.

The phosphate breakthrough curve can be subdivided into two stages. During the first stage (0−40 pore volumes), phosphate concentrations in the column effluent remained below detection (<0.01 mg P/L). During the second stage of the breakthrough curve (40−1450 pore volumes), $PO_4$ concentrations increased but remained low relative to the input concentration. The average percent breakthrough ($C/C_o$) observed during this period was 7.9% ± 6.1% ($n$ = 151) corresponding to absolute concentrations of 0.27 ± 0.20 mg/L $PO_4$−P, giving an average $PO_4$ reduction of >90%.

**Major Ion Chemistry and Speciation Modeling.** The geochemical speciation model, MINTEQA2 (*20*), was used to calculate the saturation indices of $PO_4$-bearing phases. The MINTEQA2 database was modified to make it consistent with the WATEQ4F database (*21*). This database was further modified to include additional crystalline phosphate phases for which thermodynamic data are available (Table 2). The general order of increasing solubility of the calcium phosphate phases under neutral to alkaline pH conditions is as follows: hydroxyapatite (HAP) [$Ca_5(PO_4)_3OH$], $\beta$-tricalcium phosphate (TCP) [$\beta Ca_3(PO_4)_2$], octacalcium phosphate (OCP) [$Ca_8H_2(PO_4)_6 \cdot 5H_2O$], monetite [$CaHPO_4$], and brushite [$CaHPO_4 \cdot 2H_2O$] (*22*−*24*).

An important limitation in performing thermodynamic calculations for the calcium phosphate system is that as a group these solids possess unique properties that make precise solubility determinations difficult. Often, precipitation of Ca−$PO_4$ is dominated by kinetically limited or nonequilibrium processes. The formation of metastable precursors, ionic strength and foreign ion effects, nonstoichiometry, slow crystal growth kinetics, and incongruent

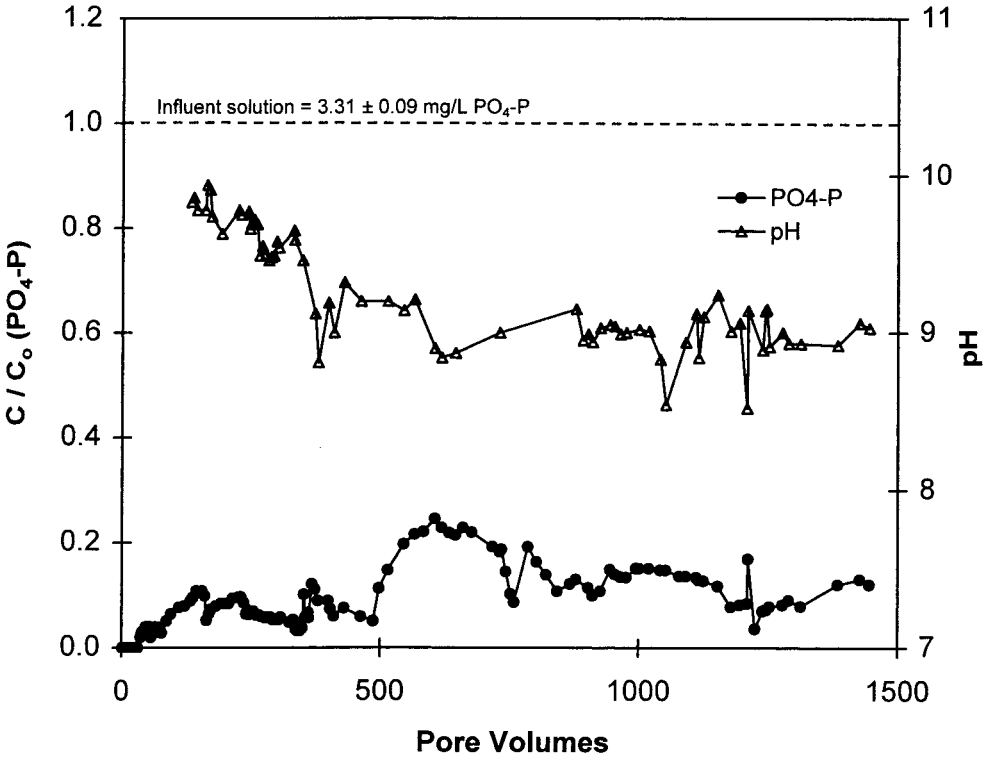


**FIGURE 3. Column 1 breakthrough curves. $C/C_o$ ($PO_4$−P) and pH versus total pore volumes of treatment.**

**TABLE 2. Calcium Phosphate Mineral Phases and Literature $K_{sp}$ Values Used during MINTEQA2 Modeling[a]**

| mineral | reaction | log $K_{sp}$ |
|---|---|---|
| calcium phosphates[b] | | |
| hydroxyapatite | $Ca_5(PO_4)_3OH + H^+ = 5Ca^{2+} + 3PO_4^{3-} + H_2O$ | −44.20 |
| | | −40.41 |
| octacalcium phosphate | $Ca_8H_2(PO_4)_6{\cdot}5H_2O = 8Ca^{2+} + 5H_2O + 6PO_4^{3-} + 2H^+$ | −93.95 |
| tricalcium phosphate (whitlockite) | $\beta Ca_3(PO_4)_2 = 3Ca^{2+} + 2PO_4^{3-}$ | −28.94 |
| brushite | $CaHPO_4{\cdot}2H_2O = Ca^{2+} + PO_4^{3-} + 2H_2O + H^+$ | −18.91 |
| monetite | $CaHPO_4 = Ca^{2+} + PO_4^{3-} + H^+$ | −19.24 |

[a] Two $K_{sp}$ values are listed for hydroxyapatite to account for the range of reported values. [b] Modified after Viellard and Yves (*23*).

dissolution all can affect the rate of crystallization as well as the specific phases that form (*24*, *25*).

The reactive mixture maintained conditions that favored the precipitation of calcium phosphate. The effluent pH decreased gradually from 9.8 at 134 pore volumes to between 8.5 and 9.3 at the conclusion of the experiment. Maintaining high pH is essential for P treatment by calcium phosphate precipitation, as calcium phosphate solubility decreases sharply with increasing pH. The column effluent remained at or near saturation with respect to calcite and slightly undersaturated with respect to dolomite. These observations suggest that calcite dissolution is an important reaction buffering the pH of the input solution over the long term. The high initial pH demonstrated in the batch experiments suggests that dissolution of portlandite and periclase dominated the pH only at early time. The final pH plateau of 8.5−9.3 is high and suggests that additional mineral phases in the BOF-oxide may be contributing to the high pH. Calcium concentrations increased from 3.5 to 6.8 mg/L as pH decreased, and Fe concentrations remained below detection (<0.01 mg/L) throughout the experiment (Figure 4). Total alkalinity values remained steady at 23.8 ± 3.0 mg/L (as $CaCO_3$). Dissolved trace metals (i.e., Pb, Cu, Zn, Ni, Co, Al) remained near or below detection limits (≈0.01 mg/L) for all major sampling events. The potential for release of trace elements may be low due to the stability of the phases contained in the BOF-oxide.

The column effluent solution remained supersaturated with respect to the least soluble calcium phosphate phase, HAP (Figure 4). Although HAP is thermodynamically stable, supersaturated conditions are commonly reported (*26*, *27*). The discrepancy between observed IAP values and levels predicted based on solubility data is attributed to the low $K_{sp}$ values used for stoichiometric, well-crystalline HAP ($K_{sp} = ([Ca]^5[PO_4^{3-}]^3)/[H^+]) = 10^{-41}-10^{-44}$). Freshly precipitated Ca−$PO_4$ has been described as an amorphous calcium phosphate (ACP) that transforms to crystalline HAP over time (*28*). A thermodynamic expression that has been reported to describe phosphate concentrations in calcite-saturated systems is that of the more soluble $\beta$-tricalcium phosphate (TCP) (*27*, *29*). The effluent from column 1 remained at or near saturation with respect to TCP. Although this solubility expression appears to best describe the observed phosphate concentrations, to the best of the our knowledge it has never been positively identified in soil systems. The column effluent remained well undersaturated with respect to the more soluble octacalcium phosphate (OCP), brushite, and monetite.

Assuming the long-term $PO_4$ concentrations exiting the column are limited by the precipitation of a discrete mineral, several interpretations of the breakthrough curve can be presented. First, the column is supersaturated with respect to crystalline hydroxyapatite, and thus phosphate concentrations are being controlled by a more soluble Ca−$PO_4$ phase.

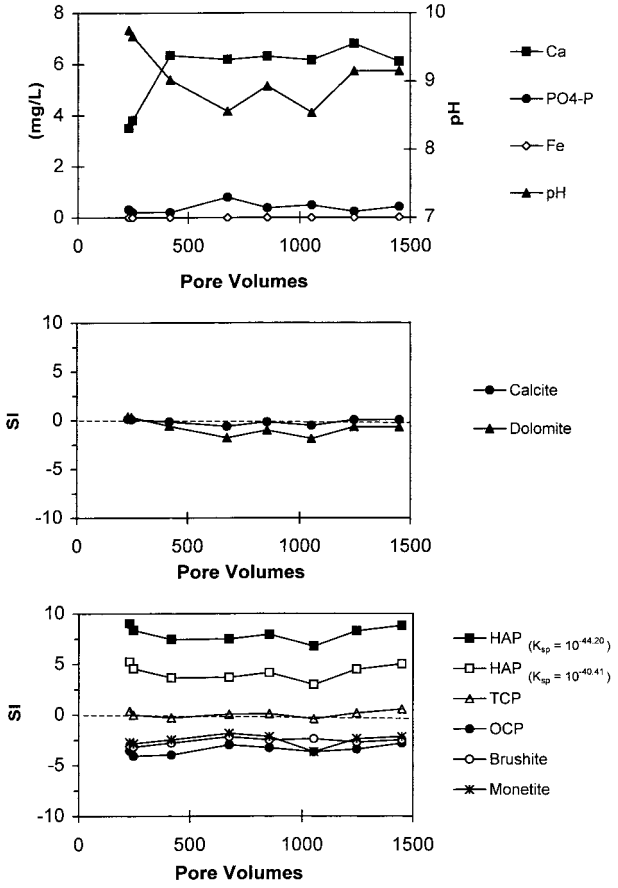


**FIGURE 4. Results of detailed sampling of column 1 effluent. Saturation indices for carbonate and Ca−$PO_4$ phases are calculated using MINTEQA2.**

Solution effects may cause these supersaturated conditions. $Mg^{2+}$ ions have been reported to stabilize early formed phases such as TCP but inhibit the nucleation of more crystalline phases such as OCP, and HAP (*24*, *30*). Despite the high Mg content of the solid phases in the column, the Mg/Ca molar ratio in the effluent water was low and decreased to a minimum of 0.1 during the experiment. Alternatively, HAP, the most stable form of calcium phosphate, is the controlling phase, and the thermodynamic $K_{sp}$ value for crystalline stoichiometric HAP is not representative of HAP forming in the column.

**Mineralogical Analyses.** Solids were extracted from both the influent and effluent ends of the column after 354 and 758 pore volumes of treatment. After 354 pore volumes, the influent end (0−1.5 cm) contained 608 $\mu$g of P/g, and the effluent end (18.5−20 cm) contained 26 $\mu$g of P/g. After 758 pore volumes of treatment, the influent end (1.5−2.5 cm) contained 232 $\mu$g of P/g, and the effluent end (17.5−18.5 cm) contained 60 $\mu$g of P/g. This distribution indicates that a zone containing a high P concentration is located at the base of the column and is advancing slowly in the direction of flow.

Mineralogical analyses were conducted on samples collected from the influent end of the column. X-ray maps of the Pk$\alpha$ wavelength were used to qualitatively identify phases on which phosphate is preferentially accumulating. Phosphorus was not associated with magnetite, the primary iron oxide phase in the BOF material. Maghemite ($\gamma$-$Fe_2O_3$) was positively identified and appears to have formed by the oxidative alteration of magnetite. Phosphorus accumulations were identified on the maghemite grains. The gradual oxidation of original magnetite grains to maghemite may provide additional adsorption capacity over time. Phosphorus was also concentrated on unidentified silt-sized spheres of iron/calcium oxide that display complex internal structures. The highest concentrations of phosphorus were found associated with the finest fraction of the BOF-oxide, which tends to adhere to the larger quartz and calcite grains (Figure 5A). The fine-grained fraction is an aggregate material composed

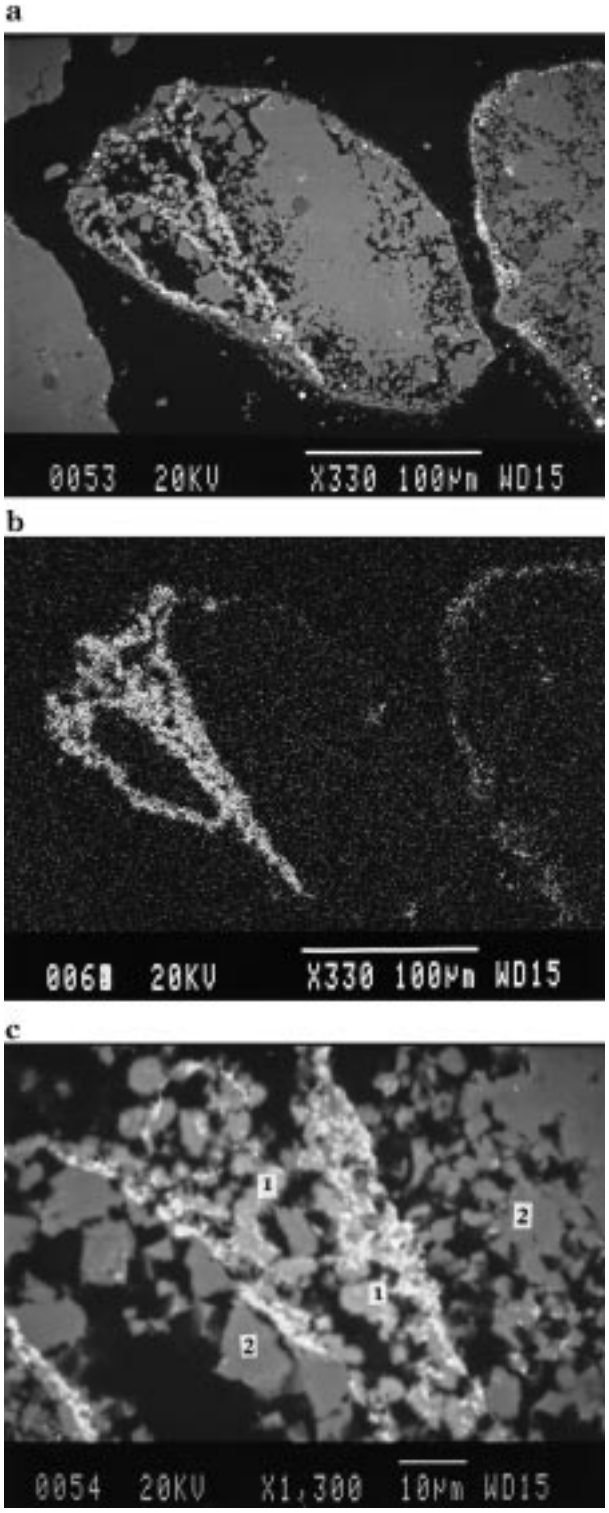


**FIGURE 5. SEM micrographs of column 1 solids. Panel A, calcite grain (gray) with thin surface coating of iron oxide (white). Panel B, X-ray map showing P distribution (corresponding to panel A). Panel C, magnified view of P-enriched area; 1, hydroxyapatite (HAP); 2, calcite.**

**TABLE 3. Apparent Solubility Calculations for Hydroxyapatite [$Ca_5(PO_4)_3OH$] Precipitate Formed in Column 1**

dissolution reaction: $Ca_5(PO_4)_3OH + H^+ = 5Ca^{2+} + 3PO_4^{3-} + H_2O$

| | | log (activity) | | | |
|---|---|---|---|---|---|
| sample | pore vol | $[Ca^{2+}]$ | $[PO_4^{3-}]$ | $[H^+]$ | log $K_{sp}$ (measd) |
| PR5-57 | 231 | −4.156 | −8.044 | −9.750 | −35.16 |
| PR5-62 | 248 | −4.111 | −8.311 | −9.660 | −35.83 |
| PR5-95 | 418 | −3.867 | −8.810 | −9.020 | −36.75 |
| PR5-109 | 675 | −3.873 | −8.629 | −8.560 | −36.70 |
| PR5-120 | 853 | −3.871 | −8.609 | −8.930 | −36.25 |
| PR5-135 | 1053 | −3.874 | −8.865 | −8.540 | −37.42 |
| PR5-149 | 1247 | −3.843 | −8.614 | −9.150 | −36.06 |
| PR5-158 | 1450 | −3.895 | −8.351 | −9.150 | −35.38 |

**Aqueous Complexes Accounted for within the MINTEQA2 Database**

| component | species | component | species |
|---|---|---|---|
| $PO_4^{3-}$ | $H_3PO_4^0$, $H_2PO_4^-$, $HPO_4^{2-}$, $PO_4^{3-}$ | $Mg^{2+}$ | $MgH_2PO_4^+$, $MgHPO_4^0$, $MgPO_4^-$ |
| $Ca^{2+}$ | $CaH_2PO_4^+$, $CaHPO_4^0$, $CaPO_4^-$ | $K^+$ | $KHPO_4^-$ |

of tiny spheres of magnetite, laths of red hematite, and other unidentified (nonopaque) iron oxide phases. Interestingly, phosphorus was concentrated in regions where calcite grains were coated with the fine-grained iron oxide material but not noncoated calcite. Hamad and Syers (*31*) suggest that the adsorption of phosphate on natural calcite is dominated by iron oxide impurities.

Microcrystalline calcium phosphate was positively identified in areas where fine BOF-oxide material was present as a coating on the surfaces of fine-grained calcite (Figure 5B,C). The precipitate may have formed by replacing calcite. This is consistent with the current understanding of the calcium phosphate system where nucleation and crystal growth are rate-limiting steps and HAP is more easily formed on existing reactive surfaces (*24*). Lack of sufficient reactive surfaces may explain supersaturated conditions with respect to HAP in natural calcareous sands (*3*). Repeated quantitative microprobe analyses on similar grains produced a mean Ca:P molar ratio of 1.72. This ratio coincides closest with the structural formula for hydroxyapatite (Ca:P = 1.67) and is distinctly different than the ratios corresponding to other potentially formed calcium phosphate phases, e.g., amorphous calcium phosphate (Ca:P = 1.30−1.50, (*28*, *30*, *32*, *33*), OCP (Ca:P = 1.33), TCP (Ca:P = 1.50), and brushite and monetite (Ca:P = 1.0).

The structural formula of hydroxyapatite was combined with the chemical analyses of column 1 effluent to calculate the apparent solubility of hydroxyapatite in this system, assuming equilibrium conditions. Activities for the ion activity product of hydroxyapatite were obtained using MINTEQA2. The formation reaction and solubility product of hydroxyapatite is given by

$$Ca_5(PO_4)_3OH + H^+ = 5Ca^{2+} + 3PO_4^{3-} + H_2O \quad (2)$$

$$K_{sp} = \frac{[Ca^{2+}]^5[PO_4^{3-}]^3}{[H^+]} \quad (3)$$

The results of the apparent solubility calculations are given in Table 3. The log(IAP) values calculated range from −35.16 to −37.42 with a mean value and 95% confidence interval of $-36.31 \pm 0.68$. This value can be used to define a provisional solubility product $K_{sp}$* for the microcrystalline phase formed in the column of $-36.31 \pm 0.68$. The value reported here is 6−10 orders of magnitude greater than the literature $K_{sp}$ values for HAP (Table 2).

**Column 2.** The reactive mixture in column 2 contained 50 wt % silica sand, 40 wt % crushed limestone, and 10 wt % AA400G activated aluminum oxide. The profile of the tracer test was highly dispersed with significant tailing in both the early and late portions of the curve. The best modeled fit yielded an effective porosity of 0.54. The high internal porosity and surface area of the activated alumina may be responsible for the dispersed tracer test profile. Therefore, using a porosity value of 0.54 (pore volume = 262 $cm^3$) provides a conservative estimate of $PO_4$ breakthrough. The

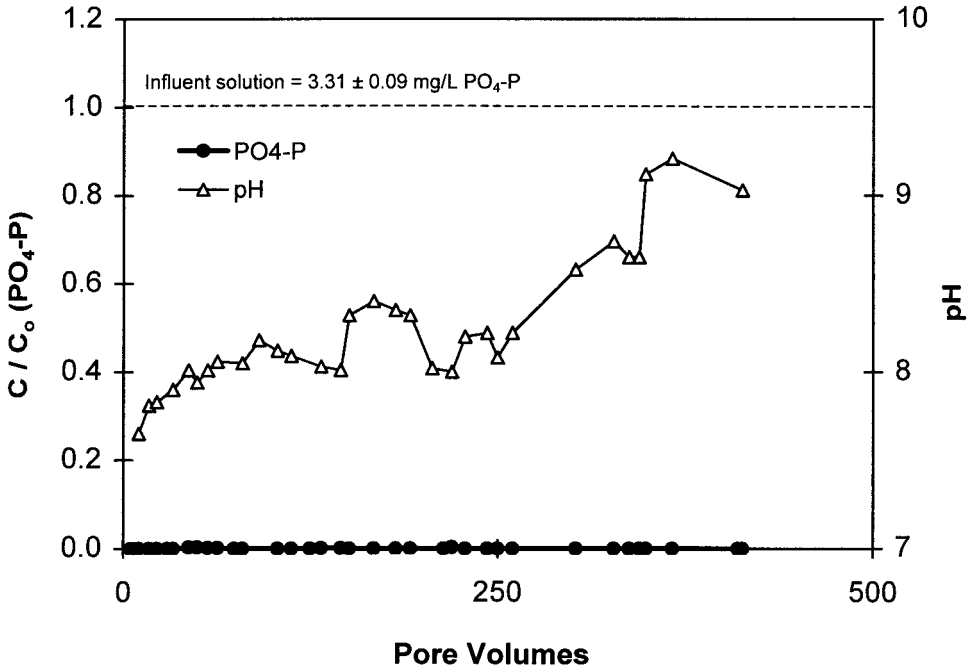


**FIGURE 6. Column 2 breakthrough curves. $C/C_o$ ($PO_4$ − P) and pH versus total pore volumes of treatment.**

velocities for column 2 averaged 9.0 ± 0.5 cm/day, giving a dimensionless flow rate of 0.6 ± 0.04 pore volume/day and an average residence time in the column of 1.7 ± 0.10 day. The $KH_2PO_4$ orthophosphate input solution was administered for a continuous period of 2.0 years or 413 pore volumes. The breakthrough curves for $PO_4$−P and pH for column 2 are shown in Figure 6.

Phosphate concentrations in the effluent remained at or below the detection limit (≤0.01 mg/L $PO_4$−P) throughout the experiment. This response is attributed to the high anion adsorption capacity of the activated aluminum, despite the relatively high pH (≈8−9) of the column porewater. Assuming that the $PO_4$ reductions are due only to adsorption, then a minimum adsorption capacity ($M_p$) under dynamic flow conditions can be calculated, where $M_p$ = mg of P removed/kg of solids. The adsorption capacity was 452 mg of P/kg (reactive mixture). If it is further assumed that P adsorption is dominated by the aluminum oxide, then the minimum adsorption capacity for the AA400G activated aluminum is $M_p$ = 4531 mg of P/kg of oxide. These are considered minimum values as the adsorption capacity has not yet been fully utilized thus far in the experiment. In comparison, Aitkens (*34*) conducted a survey of phosphate adsorption capacities of soil and sediment samples from the Canadian Shield using a Langmuir isotherm approach. The mean adsorption capacity of these natural soils and sediments was 113.2 mg of P/kg, with a minimum of 6.3 mg of P/kg and a maximum of 501.0 mg of P/kg.

Due to the absence of any detectable phosphate breakthrough in column 2, geochemical modeling of the effluent and calculation of saturation indices was not performed. Activated alumina may be a useful material in situations where very high treatment efficiencies are required or in specific applications in which the mixture can be easily replaced when the adsorption capacity is exceeded. However, the cost of high capacity adsorbents such as activated alumina may be prohibitive.

Column experiments have demonstrated effective levels of long-term phosphorus treatment with reactive mixtures at an application rate of approximately 1 pore volume/day. The reactive mixtures used here provided a geochemical environment for both $PO_4$ adsorption on surfaces of metal oxides and precipitation of sparingly soluble calcium phosphate.

## Acknowledgments

The authors wish to thank J. L. Jambor for performing the mineralogical analyses.

## Literature Cited

(1) Whilhelm, S. R.; Schiff, S. L.; Cherry, J. A. *Ground Water* **1994**, *32*, 905−916.
(2) McMaster, M. L.; Trevors, K. E. *Waterloo Centre for Groundwater Research Annual Septic System Conference*, Waterloo, ON, May 15; 1995; pp 99−104.
(3) Robertson, W. D. *J. Contam. Hydrol.* **1995**, *19*, 289−305.
(4) Walter, D. A.; Rea, B. A.; Stollenwerk, K. G.; Savoie, J. *U.S. Geol. Surv. Water-Supply Pap.* **1996**, *No. 2463*.
(5) Schindler, D. W. *Science* **1977**, *195*, 260−262.
(6) Brooks, J. L.; Rock, C. A.; Struchtemer, R. A. *J. Environ. Qual.* **1984**, *13*, 524−530.
(7) Chowdhry, N. A. *Water Pollut. Control* **1975**, 17−18.
(8) Blowes, D. W.; Ptacek, C. J.; Baker, M. J. Treatment of phosphorus in water. U.K. patent application no. 9523113.0, 1995.
(9) Baker, M. J.; Blowes, D. W.; Ptacek, C. J. *Land Contam. Reclam.* **1997**, *5*, 189−193.
(10) Loudon, T. L. *Waterloo Centre for Groundwater Research Annual Septic System Conference*, Waterloo, ON, May 13; 1996; pp 4−11.
(11) Jowett, E. C.; McMaster, M. L. *J. Environ. Qual.* **1995**, *24*, 86−95.
(12) Goldberg, S.; Sposito, G. *Commun. Soil Sci. Plant Anal.* **1985**, *16*, 801−821.
(13) Nriagu, J. O. In *Phosphate Minerals*; Nriagu, J. O., Moore, P. B., Eds.; Springer-Verlag: New York, 1984; pp 1−136.
(14) Mikhail, S. A.; Owens, D. R.; Wang, S. S. B.; Lastra, R.; Van Huyssteen, E. Technology Report No. 94-18. MSL Project 691; Canmet: Ottawa, ON, 1994; 41 pp.
(15) *Standard Methods for the Examination of Water and Wastewater*, 18th ed.; Greenberg, A. E., Cleceri, L. S., Eaton, A. D., Eds.; American Health Association: Washington, DC, 1992.
(16) Mayer, T. Technical Report to the Rivers Research Branch, National Water Research Institute, Burlington, ON, 1981; 13 pp.
(17) Freeman, J. S.; Rowell, D. L. *J. Soil Sci.* **1981**, *32*, 75−84.
(18) Neufeld, R. D.; Thodos, G. *Environ. Sci. Technol.* **1969**, *3*, 661−667.
(19) Parker, J. C.; van Genuchten, M. T. Virginia Agricultural Experiment Station **1984**, *Bull. 84-3*.
(20) Allison, J. D.; Brown, D. S.; Novo-Gradac, K. J. *MINTEQA2/PRODEFA2, A Geochemical Assessment Model for Environmental Systems: Version 3.0 User's manual*; U.S. Environental Protection Agency: Athens, GA, 1990, 106 pp.
(21) Ball, J. W.; Nordstrom, D. K. *Open-File Rep.—U.S. Geol. Surv.* **1991**, *No. 91−183*, 189 pp.
(22) Brown, W. E. In *Environmental Phosphorus Handbook*; Griffith, E. J., Beeton, A., Spencer, J. M., Mitchell, D. T., Eds.; John-Wiley and Sons: New York, 1973; pp 203−239.
(23) Vieillard, P.; Yves, T. In *Phosphate Minerals*; Nriagu, J. O., Moore, P. B., Eds.; Springer-Verlag: New York, 1984; pp 171−198.
(24) Nancollas, G. H. In *Phosphate Minerals*; Nriagu, J. O.; Moore, P. B., Eds.; Springer-Verlag: New York, 1984; pp 137−154.
(25) Posner, A. S.; Blumenthal, N. C.; Betts, F. In *Phosphate Minerals*; Nriagu, J. O., Moore, P. B., Eds.; Springer-Verlag: 1984; pp 330−350.
(26) Staudinger, B.; Peiffer, S.; Avnimelech, Y.; Berman, T. *Hydrobiologic* **1990**, *207*, 167−177.
(27) Norvell, W. A. *Water Pollut. Control Fed.* **1974**, *38*, 441−445.
(28) Boskey, A.; Posner, A. S. *J. Phys. Chem.* **1973**, *77*, 2313−2317.
(29) Moore, P. A.; Reddy, K. R. J. *Environ. Qual.* **1994**, *23*, 955−964.
(30) Kibalczyc, W.; Christoffersen, J.; Christoffersen, M. R.; Zielenkiewicz, A.; Zielenkiewicz, W. *J. Cryst. Growth* **1990**, *106*, 355−366.
(31) Hamad, M. E.; Rimmer, D. L.; Syers, J. K. *J. Soil Sci.* **1992**, *43*, 273−281.
(32) Christoffersen, M. R.; Christoffersen, J.; Kibalczyc, W. *J. Cryst. Growth* **1990**, *106*, 349−354.
(33) Tropp, J.; Blumenthal, N. C.; Waugh, J. S. *J. Am. Chem. Soc.* **1983**, *105*, 22−26.
(34) Aitkens, D. F. Technical Support Section, Southeast Region, Ontario Ministry of the Environment, 1975.

*Received for review October 23, 1997. Revised manuscript received April 1, 1998. Accepted April 17, 1998.*

ES970934W